

Core–Shell Particles for Simultaneous 3D Imaging and Optical Tweezing in Dense Colloidal Materials

Yanyan Liu, Kazem V. Edmond, Arran Curran, Charles Bryant, Bo Peng, Dirk G. A. L. Aarts, Stefano Sacanna,* and Roel P. A. Dullens*

Colloidal suspensions of microspheres have been used as idealized yet accurate physical models of complex phase behaviors for over a century.^[1–4] The earliest and perhaps most significant example of colloids as atomic models is Jean Perrin's experiments from the early 1900s, where his quantitative measurements of Brownian diffusion confirmed Einstein's theory of diffusion, thereby solidifying Boltzmann's statistical mechanics.^[1] Since then, model colloidal suspensions have provided fundamental insights into a wide range of phase transitions.^[2,4] Early investigations of dense colloidal phases used light-scattering techniques to probe deep within the sample, providing a wealth of information about the material's internal structure and dynamics, but as an ensemble average.^[5,6] More recently, by using solvent mixtures that match the particles' refractive index and mass density, powerful 3D imaging techniques, such as confocal microscopy, enabled the direct real-space and time-resolved study of the colloidal material's complex structural and dynamical properties at the single particle level.^[7,8] This allowed unprecedented access to the local processes involved in condensed matter phenomena such as crystallization, glass formation, and gels.^[9–12]

Moving beyond simple observations, researchers have begun to probe colloidal materials directly by manipulating individual particles using optical tweezers.^[13,14] However, simultaneous optical manipulation and 3D visualization of dense colloidal samples poses significant technical challenges due to their conflicting requirements:^[15–19] while 3D visualization requires optical transparency, optical tweezing and manipulation requires a refractive index contrast between the “probe” particles and solvent.

A desirable solution would be a core–shell “probe” particle where the core diameter, shell thickness, and their respective refractive indices could be controlled independently. As such, the core size and refractive index could be tuned sufficiently for reliable optical trapping, yet interfering minimally with the visualization of the surrounding sample, whilst the shell's thickness could be adjusted as required yet remaining optically transparent. Although there have been numerous reports on the synthesis of core–shell particles,^[20–27] none describes how to fabricate micron-sized particles with a thick shell, appropriate for both confocal imaging and optical trapping in dense materials. Here, we introduce a simple, yet robust and general approach involving a two-step heterogeneous nucleation procedure to encapsulate a variety of different core particles within a thick uniform shell.

A commonly encountered challenge in seeded emulsion polymerization is that core particles may get kinetically trapped at the oil–water interface due to the large pinning forces involved.^[28,29] However, a recent study of seeded emulsion polymerization using 3-trimethoxysilyl propyl methacrylate (TPM)^[30] shows that at relatively low concentrations, hydrolyzed TPM (hTPM) can form evenly sized “lobes” on the surfaces of the core particles under basic conditions. These lobes can be polymerized into TPM, resulting in raspberry-shaped particles. In the fabrication procedure described herein, we repeat the seeded emulsion polymerization with TPM using the raspberry particles as “seeds”, where the nucleated TPM droplets fill the lobe interstices that, when polymerized, yield a smooth uniform TPM shell. The core size and TPM shell's thickness can be independently tuned. Most importantly, the optical contrast of the core–shell particle can be controlled by using cores of different materials, such as melamine-formaldehyde (MF), polystyrene (PS), and TPM. As such, the size and refractive index of the core can, independent to the shell-thickness, be optimized for optical tweezing.^[31] By dispersing our optical core–shell particles in a host system of fluorescently labeled TPM particles, hence ensuring identical interactions between all particles, and subsequently refractive index matching the TPM with an appropriate solvent mixture, we achieve a new colloidal system that enables simultaneous 3D confocal microscopy and optical manipulation. We demonstrate this capability by dragging a core–shell “probe” particle through a dense colloidal crystal of TPM “host” spheres using holographic optical trapping, whilst the surrounding 3D crystal is imaged at high speed by confocal microscopy.

The optical core–shell particles are synthesised using a two-stage procedure as schematically shown in **Figure 1a** (see the Experimental Section). In the first stage, a core particle is coated by a relatively low concentration of hTPM under basic condition to form evenly sized lobes on the surface of the core particle.^[30] Polymerization of the TPM lobes results in a raspberry

Y. Liu, Dr. K. V. Edmond, Dr. A. Curran, C. Bryant,
Dr. B. Peng, Prof. D. G. A. L. Aarts, Dr. R. P. A. Dullens
Department of Chemistry
Physical and Theoretical Chemistry Laboratory
University of Oxford
South Parks Road, Oxford OX1 3QZ, United Kingdom
E-mail: roel.dullens@chem.ox.ac.uk



Dr. S. Sacanna
Molecular Design Institute
Department of Chemistry
New York University
100 Washington Square East, NY 10003, USA
E-mail: s.sacanna@nyu.edu

This is an open access article under the terms of the Creative Commons Attribution License, which permits use, distribution and reproduction in any medium, provided the original work is properly cited.

The copyright line for this article was changed on 2 Aug 2016 after original online publication.

DOI: 10.1002/adma.201602137

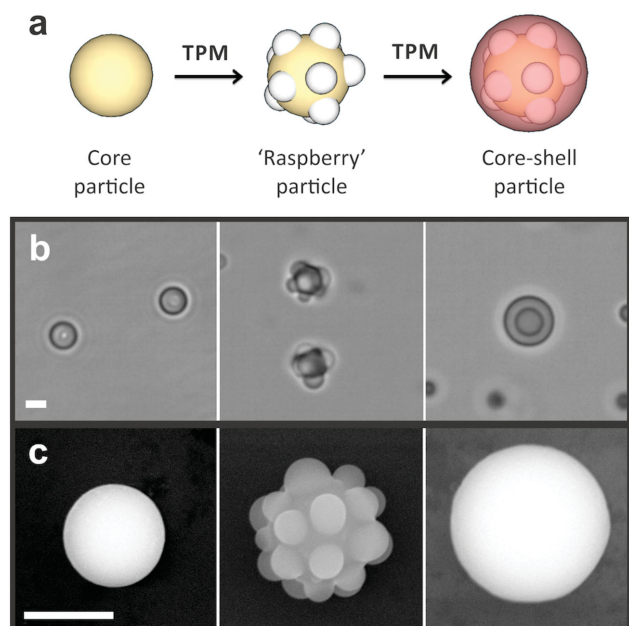


Figure 1. Principle of two-stage core-shell synthesis. a) Schematic illustrating how the first TPM coating results in a 'raspberry' particle, and the second TPM coating forms a homogeneous and concentric core-shell particle. b) Optical and c) scanning electron microscopy images of the particles in each stage, using a polystyrene (PS) core. Scale bars, 1.5 μm .

shaped particle as shown in the second illustration of Figure 1a. In the second stage, the TPM nucleates on the surface of the raspberry particle and rapidly coalesces, resulting in raspberry particles with the interstitial spaces between the lobes filled with unpolymerized TPM oil (see the Supporting Information). Provided that a sufficient quantity of hTPM is used, a thick and homogeneous TPM shell will form after radical polymerization is completed, as shown in the third illustration in Figure 1a. The different stages of the synthesis can be directly observed using brightfield microscopy, and an example from a PS-TPM core-shell synthesis is given in Figure 1b. We also observe that virtually all of the core particles are coated with TPM lobes, as shown by further images in the Supporting Information. The large shell thickness and the refractive index difference between the core and the TPM shell ensures that the core-shell structures are easily seen. The TPM shell also appears homogeneous, despite the two-stage coating procedure. It is apparent from these images that there is significant increase in the size of the particles after each stage, and this is further corroborated by the scanning electron microscopy images presented in Figure 1c.

The two-stage mechanism and core-shell morphology is furthermore demonstrated using selective fluorescent labeling of the

particle at the various stages of the synthesis. We have synthesized PS-TPM core-shell particles, where the core has been labeled with the fluorophore 4-methylaminoethylmethacrylate-7-nitrobenzo-2-oxa-1,3-diazol (NBD-NAEM, $\lambda_{\text{ex}} = 488 \text{ nm}$),^[32] and the second TPM layer is labeled with rhodamine-isothiocyanate-3-aminopropyltrimethoxysilane (RITC-APS, $\lambda_{\text{ex}} = 561 \text{ nm}$).^[32,33] No fluorophore was used during the raspberry formation stage. Figure 2a shows a confocal image where the sample is simultaneously excited with 488 and 561 nm laser light, and Figure 2b,c shows the separate detection channels for the two different fluorescent dyes. From these confocal images, the different stages are clearly distinguishable: the fluorescent PS cores, and the fluorescent outer TPM layer, which is smooth on the outside but structured on the inside due to the presence of the unlabeled lobes. Note that the red central spots in Figure 2c are caused by the strong back scattering of the high refractive index cores. To confirm the concentric nature of the core-shell particles and the homogeneity of the shell, we calcinate PS-TPM and MF-TPM core-shell particles at temperatures above 300 and 500 $^{\circ}\text{C}$ respectively. During this process the organic components of the core disintegrate, while the TPM shell decomposes into a silica rich material. Applying mechanical stress to the calcinated particles resulted in some broken, but clearly concentric and homogeneous shells, as shown in Figure 2d,e for the PS-TPM and MF-TPM core-shell particles, respectively.

Conveniently, the optical contrast between the core and shell can be adjusted by changing the core material, underlining the generality and flexibility of our approach. So far we have successfully incorporated MF ($n \approx 1.68$), PS ($n \approx 1.59$) and TPM ($n \approx 1.50$) cores (see the Supporting Information), which implies

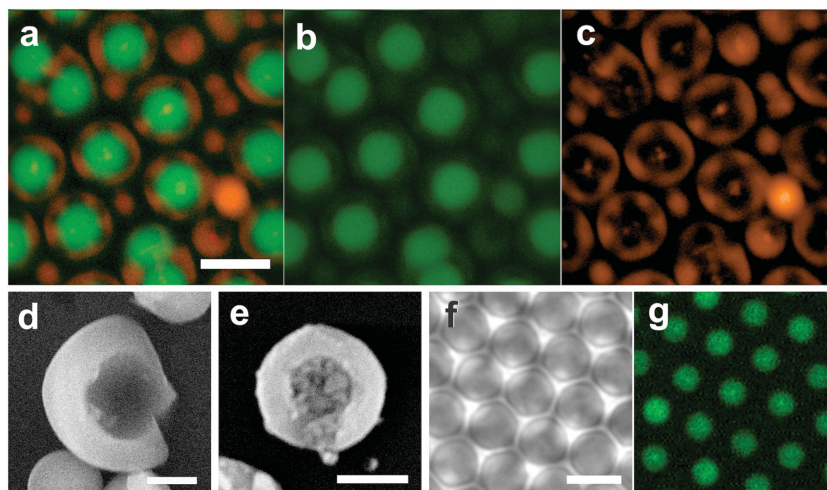


Figure 2. Selective labeling of the core and shell. a) Confocal microscopy image showing PS-TPM core-shell particles, where the cores have been labeled with NBD-NAEM and the second TPM coating with RITC-APS. The scale bar is 3 μm and also applies to (b) and (c), showing the separate detection channels. The dark regions observed in panels (a) and (c) are the unlabeled TPM lobes from the first TPM coating. Note that the smaller particles seen in between the core-shell particles are secondarily nucleated TPM particles. Scanning electron microscopy images of d) PS-TPM and e) MF-TPM core-shell particles after calcination and applying mechanical stress. The scale bars in panels (d) and (e) are 1 μm . f) Brightfield and g) confocal microscopy images of TPM-TPM core-shell particles with RITC-APS labeled TPM cores. The scale bar in panel (f) is 3 μm and also applies to panel (g).

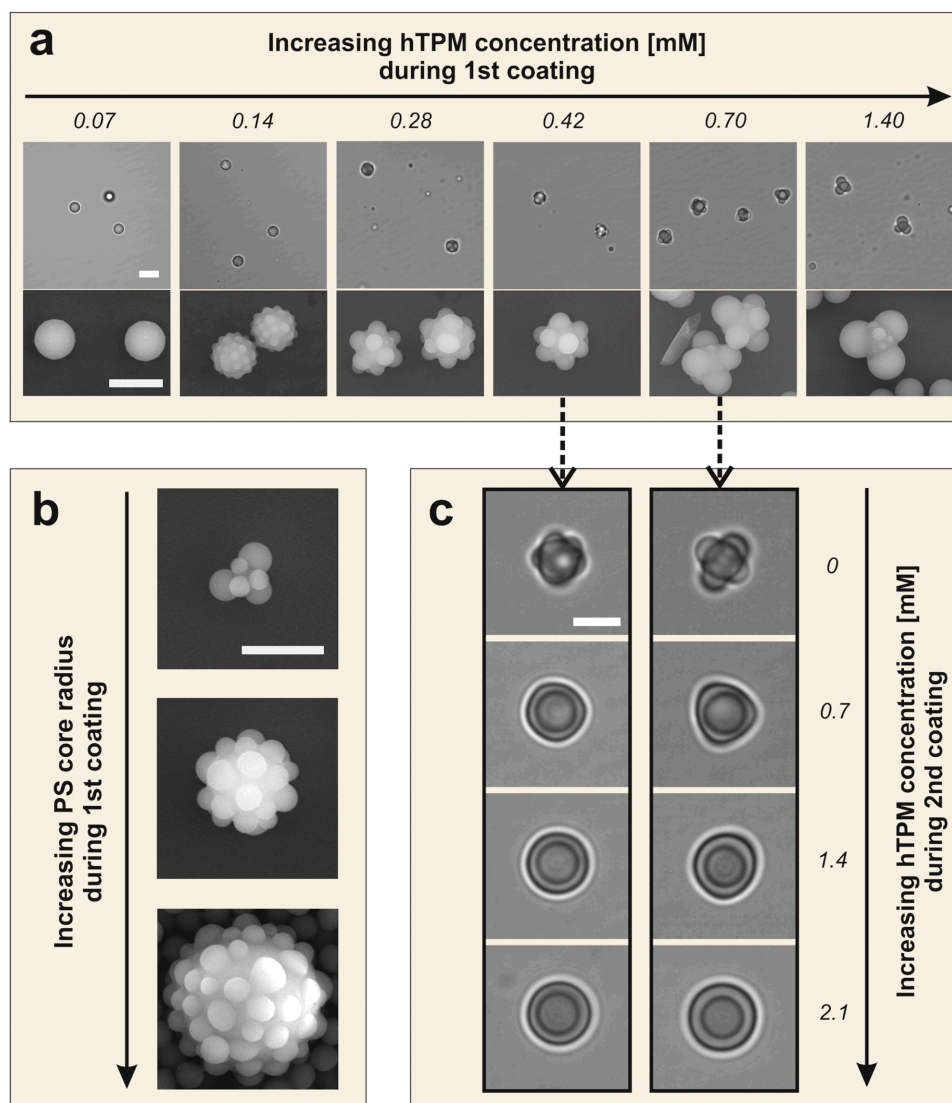


Figure 3. Controlling the shell thickness. The thickness of the shell is mostly affected by the concentration of hTPM used in the first coating stage. a) The effect of the hTPM concentration in the first coating stage on the lobe-size of the resulting raspberry particles, as observed by brightfield (top row) and scanning electron microscopy (bottom row). b) Scanning electron microscopy images of raspberry particles made by coating a batch of polydisperse PS cores at hTPM concentration of 0.42×10^{-3} M. c) The effect of the hTPM concentration in the second coating stage on the core-shell particle morphology for raspberry particles with smaller (left column) and larger (right column) lobes. All the scale bars are $3 \mu\text{m}$ and apply to the corresponding images in the same rows (a) or columns (b) and (c).

that the refractive index contrast between the core and the TPM shell can be tuned from ≈ 0.18 (MF) to 0 (TPM). As a TPM-TPM core-shell particle is compositionally identical to a homogeneous TPM particle, its core-shell nature is not observable using brightfield microscopy. However, by fluorescently labeling only the TPM cores, the core-shell structure is easily inferred from the corresponding brightfield and confocal images, as presented in Figure 2f,g, respectively. The hexagonal close packed nature of the sample means that the separation between the fluorescent cores arises solely from the presence of the non-fluorescent shell. While TPM-TPM core-shell particles are unsuitable for optical trapping when dispersed in TPM refractive index matching solvents, they are however much better for confocal imaging and tracking in dense suspensions.^[22,23]

Additionally, the size of the core and the thickness of the shell can be independently controlled, which allows to optimize the core size for optical tweezing, irrespective of the total size of the core-shell particle. In particular, we find that the final thickness of the shell is essentially controlled by the size of the raspberry lobes. As shown in Figure 3a, increasing the concentration of hTPM used in the first coating stage leads to a clear increase of the lobe-size of the resulting raspberry particles. In contrast, the lobe-size does not significantly depend on the core-size for a given concentration of hTPM within the range of core particle concentrations typically used in the first coating stage (10^8 – 10^{10} particles mL^{-1}). This is illustrated in Figure 3b, where we show raspberry particles with different core sizes obtained after coating a batch of polydisperse PS cores with TPM once.

Figure 3c shows the effect of varying the hTPM concentration in the second coating stage on the morphology of the final core-shell particle for raspberry particles with two different lobe-sizes. We find that the effect of increasing the hTPM concentration in the second coating stage is limited to affecting the surface roughness of the resulting core-shell particle. For the raspberry particle with the smaller lobes (left column in Figure 3c), a smooth core-shell particle with a shell thickness of ≈ 600 nm is achieved at a hTPM concentration of 1.4×10^{-3} M. In comparison, for the raspberry particle with the larger lobes (right column in Figure 3c), a hTPM concentration of 2.1×10^{-3} M is required to obtain a smooth core-shell particle with a shell thickness of ≈ 800 nm. At insufficient hTPM concentrations, the lobes protrude the second TPM layer resulting in a rough surface. Therefore, to produce smooth and spherical core-shell particles, the hTPM concentration in the second coating stage needs to be sufficiently high to fill all the interstitial space between the lobes.

We have characterized the optical properties of the core-shell particles using in-line digital holographic microscopy^[34] (see the Supporting Information). Figure 4 shows experimental holograms for (a) TPM, (b) PS-TPM and (c) MF-TPM core-shell particles in water. Using the Python module HoloPy,^[35] we have computed fits for each hologram (see the Supporting Information), which are shown as insets in Figure 4a–c. The resulting values for the radius of the cores, thicknesses of the shell, and

the refractive indices of these are provided in Table S1 (Supporting Information). In all cases, we are able to fit our experimental data well, which further confirms the concentric nature of the core-shell particles as well as the homogeneous thickness of the TPM shells.

Ultimately, our goal is to produce a refractive index-matched colloidal suspension of TPM particles, which requires transferring the particles from an aqueous solution, where they are synthesized, to a solvent mixture that closely matches the refractive index of TPM. To this end, we disperse the particles in a binary solvent mixture of 40/60 (v/v) trichloroethylene and tetralin ($n \approx 1.517$, see the Supporting Information), which very nearly matches the TPM's refractive index (Table S2, Supporting Information) and is close to the particle density ($\rho \approx 1.29$ g mL⁻¹). We use a commercial dispersant OLOA 1200 to tune the electrostatic screening length between the particles.^[36] Detailed descriptions of the formulation of the solvent mixture, the measurement of the refractive index, and the stabilization with OLOA are provided in the Supporting Information. Next, we optically trap MF-TPM and PS-TPM core-shell particles dispersed in this refractive index matching binary solvent mixture. The corresponding trapping potentials are shown in Figure 4d. In the same figure, we also show the trapping potential for the MF core, which, importantly, is nearly identical to the trapping potential of the MF-TPM core-shell particle. This agreement thus quantitatively confirms the near perfect refractive index matching of the TPM shell by our binary solvent mixture.

Finally, to demonstrate the simultaneous 3D imaging and optical trapping capability of our new colloidal system, we drag an individual core-shell “probe” particle along a complex 3D trajectory through a dense, refractive index matched colloidal crystal of fluorescent TPM “host” particles. To this end, we adjust the solvent mixture's ratio to introduce a very slight density mismatch, gradually sedimenting the particles and allowing for the formation of large colloidal crystals, while still maintaining good optical clarity for quantitative 3D confocal imaging deep within the sample. Using our hybrid optical trapping – confocal microscopy setup,^[16] we optically trap a PS-TPM core-shell particle and drag it through the colloidal crystal following a sinusoidal trajectory along a circular orbit, while simultaneously imaging the system in 3D using high-speed confocal microscopy, demonstrating independent control in all three directions. In Figure 5 we show the region of the colloidal crystal around the probe particle's trajectory, including a 3D reconstruction of the confocal data (a), a computer-generated rendering of the particle coordinates (b), and time-projections of different cross-sections showing the position of the probe along its full trajectory (c–e). We track each host particle over time individually in 3D using standard tracking routines,^[37] drawing their coordinates (at $t = 0$ s) as computer-generated spheres in Figure 5b. The position of the probe particle's at different times is depicted as a black circle in Figures 5c–e, which are projections over time for the minimum pixel values within each frame. In the Supporting Information, we provide a video of the confocal data that shows the probe particle as it is dragged through the colloidal crystal. These experiments clearly demonstrate the capability of our colloidal system for simultaneous optical manipulation and quantitative 3D confocal microscopy in dense colloidal materials. This for instance

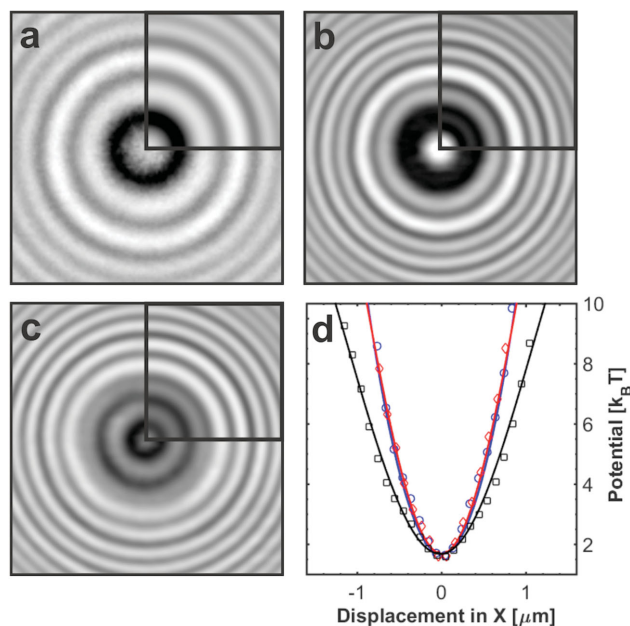


Figure 4. Digital holographic microscopy and optical tweezing of core-shell particles. Digital holographic microscopy images of a) a TPM particle, b) a PS-TPM core-shell particle, and c) a MF-TPM core-shell particle in water. Insets (upper right quadrants): fitted holograms using HoloPy,^[34] with all fitting parameters provided in Table S1 (Supporting Information). d) Optical trapping potentials for a MF particle (\diamond), a MF-TPM core-shell particle (\circ), and a PS-TPM core-shell particle (\square) in a refractive index matching binary solvent mixture of 40/60 (v/v) trichloroethylene–tetralin (Table S2, Supporting Information). The solid lines are fits according to a parabolic potential kx^2 and the trapping stiffnesses are: $k_{MF} = 9.6 \mu\text{N m}^{-1}$, $k_{MF-TPM} = 9.7 \mu\text{N m}^{-1}$ and $k_{PS-TPM} = 5.9 \mu\text{N m}^{-1}$.

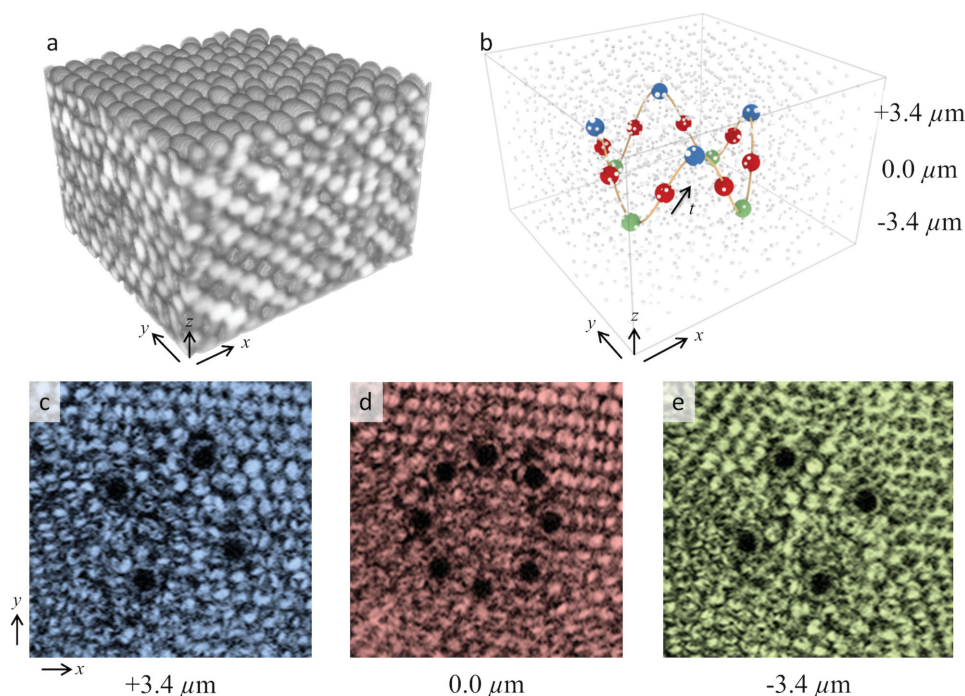


Figure 5. Simultaneous 3D imaging and optical tweezing of a core-shell particle in a colloidal crystal. a) 3D reconstruction of confocal data from sample's region of interest. b) Computer-generated image of actual particle coordinates. White/gray particles are the background "host" particles at the initial time, drawn smaller for clarity. The core-shell "probe" particle is drawn at its maximum and minimum z-position for its full trajectory, depicted larger and with contrasting colors for clarity. The probe's trajectory is drawn in orange. c–e) Time projections of minimum pixel values for three cross-sections within the region of interest, showing the probe's locations at c) "top", d) "middle", and e) "bottom" of its trajectory. See the Supporting Information for a video of the confocal data.

enables the direct measurement of Zener pinning,^[38] which plays a significant role in materials processing, having a strong influence on recovery, recrystallization, and grain growth.^[39]

In summary, we have described the development of novel micro-sized core-shell particles that enable simultaneous 3D confocal imaging and optical tweezing by embedding them as "probe" particles in a dense and optically matched "host" suspension of fluorescently labeled particles. While the probe's core is made of a high refractive index material, the probe's shell and surrounding host particles are both made of TPM, which can be refractive index and density matched by a mixture of organic solvents, rendering them invisible to the optical tweezer. The core-size and shell-thickness can be independently tuned and we have further shown the generality and flexibility of our approach by incorporating cores made of melamine formaldehyde, polystyrene, and TPM. By dragging a core-shell particle through a dense colloidal crystal, we have demonstrated the unique capability of our new colloidal system for performing quantitative 3D confocal imaging while simultaneously optically trapping, a capacity which we believe will open up a broad range of opportunities to address many outstanding problems in condensed matter science.

Experimental Section

The core-shell particles were fabricated by nucleating and polymerizing TPM oil on the surface of the core particles (the synthesis of the various core particles is described in the Supporting Information). In a 30 mL

glass vial, a solution of hydrolyzed TPM oil (hTPM) was prepared by stirring TPM oil in water at a 1:30 (v/v) ratio with a magnetic stir-bar overnight. In a typical 30 mL reaction (pH \approx 10), core particles ($\approx 10^8$ particles mL⁻¹), 30 μ L NH₃ (30–33 wt%, as received), and 2 mL hTPM solution were mixed well with water. The reaction mixture was then covered and left undisturbed for 30 min before \approx 50 mg azobisisobutyronitrile (AIBN) was added, then transferred to a sealed 30 mL glass bottle and placed in a preheated 75 °C oven for 5 h to be polymerized. The product particles were cleaned in water by repeated centrifugation at 800 rpm, decanting, and redispersion by gentle sonication and stirring. Any secondary TPM nuclei were removed by repeatedly decanting the solution at least three times. The size of the raspberry lobes can be tuned by adjusting the concentration of hTPM solution added initially. Similarly, in the second TPM coating stage, raspberry particles ($\approx 10^5$ particles mL⁻¹) were mixed in a 30 mL aqueous reaction mixture containing 30 μ L NH₃ and 5 mL hTPM solution. The final TPM shell was polymerized as before: the reaction mixture was covered, left undisturbed for 30 min, \approx 50 mg AIBN was added, and the solution was then transferred to a sealed 30 mL glass bottle and placed in a preheated 75 °C oven for 5 h. The resulting core-shell particles were cleaned in water by repeated centrifugation, decanting, and redispersion, as described above. Any secondary TPM particles were, as before, removed by repeated decanting.

Further experimental details on the synthesis of the TPM host particles, digital holographic microscopy, refractive index matching, and solvent transfer are given in the Supporting Information.

Supporting Information

Supporting Information is available from the Wiley Online Library or from the author.

Acknowledgements

The authors thank Theodore Hueckel, Joseph Auslander, Vinothan Manoharan, and David Grier for useful discussions, and Eric Dufresne for providing the OLOA 1200 reagent. This work was supported by the European Research Council (ERC Starting Grant No. 279541-IMCOLMAT) and the EPSRC (Grant No. EP/J001902/1).

Received: April 22, 2016

Revised: June 6, 2016

Published online: July 5, 2016

- [1] J. Perrin, *Atoms*, D. Van Nostrand Co., New York, USA **1916**.
- [2] P. N. Pusey, W. van Megen, *Nature* **1986**, 320, 340.
- [3] G. L. Hunter, E. R. Weeks, *Rep. Prog. Phys.* **2012**, 75, 066501.
- [4] W. Poon, H. Lekkerkerker, *Phys. World* **1996**, 9, 27.
- [5] P. N. Pusey, W. van Megen, *Phys. Rev. Lett.* **1987**, 59, 2083.
- [6] W. van Megen, P. N. Pusey, *Phys. Rev. A* **1991**, 43, 5429.
- [7] A. van Blaaderen, P. Wiltzius, *Science* **1995**, 270, 1177.
- [8] V. Prasad, D. Semwogerere, E. R. Weeks, *J. Phys.: Cond. Matt.* **2007**, 19, 113102.
- [9] W. K. Kegel, A. van Blaaderen, *Science* **2000**, 287, 290.
- [10] E. R. Weeks, J. C. Crocker, A. C. Levitt, A. Schofield, D. A. Weitz, *Science* **2000**, 287, 627.
- [11] U. Gasser, E. R. Weeks, A. B. Schofield, P. N. Pusey, D. A. Weitz, *Science* **2001**, 292, 258.
- [12] P. J. Lu, E. Zaccarelli, F. Ciulla, A. B. Schofield, F. Sciortino, D. A. Weitz, *Nature* **2008**, 453, 499.
- [13] A. Ashkin, J. M. Dziedzic, J. E. Bjorkholm, S. Chu, *Opt. Lett.* **1986**, 11, 288.
- [14] D. G. Grier, *Nature* **2003**, 424, 810.
- [15] D. L. J. Vossen, A. van der Horst, M. Dogterom, A. van Blaaderen, *Rev. Sci. Instrum.* **2004**, 75, 2960.
- [16] A. Curran, S. Tuohy, D. G. A. L. Aarts, M. J. Booth, T. Wilson, R. P. A. Dullens, *Optica* **2014**, 1, 223.
- [17] M. Yevnin, D. Kasimov, Y. Gluckman, Y. Ebenstein, Y. Roichman, *Biomed. Opt. Express* **2013**, 4, 2087.
- [18] M. Hermes, E. C. M. Vermolen, M. E. Leunissen, D. L. J. Vossen, P. D. J. van Oostrum, M. Dijkstra, A. van Blaaderen, *Soft Matter* **2011**, 7, 4623.
- [19] W. T. M. Irvine, V. Vitelli, P. M. Chaikin, *Nature* **2010**, 468, 947.
- [20] F. Caruso, *Adv. Mater.* **2001**, 13, 1.
- [21] M. S. Fleming, T. K. Mandal, D. R. Walt, *Chem. Mater.* **2001**, 13, 2210.
- [22] R. P. A. Dullens, Claesson, D. Derks, A. van Blaaderen, W. K. Kegel, *Langmuir* **2003**, 19, 5963.
- [23] M. T. Elsesser, A. D. Hollingsworth, K. V. Edmond, D. J. Pine, *Langmuir* **2011**, 27, 917.
- [24] T.-S. Deng, F. Marlow, *Chem. Mater.* **2011**, 24, 536.
- [25] R. Pelton, *Adv. Colloid Interface Sci.* **2000**, 85, 1.
- [26] W. Schärfl, *Adv. Mater.* **2000**, 12, 24.
- [27] A. Perro, G. Meng, J. Fung, V. N. Manoharan, *Langmuir* **2009**, 25, 11295.
- [28] S. U. Pickering, *J. Chem. Soc. Trans.* **1907**, 91, 2001.
- [29] D. M. Kaz, R. McGorty, M. Mani, M. P. Brenner, V. N. Manoharan, *Nat. Mater.* **2012**, 11, 138.
- [30] S. Sacanna, M. Korpics, K. Rodriguez, L. Colón-Meléndez, S.-H. Kim, D. J. Pine, G.-R. Yi, *Nat. Commun.* **2013**, 4, 1688.
- [31] T. A. Nieminen, V. L. Y. Loke, A. B. Stilgoe, G. Knöner, A. M. Brańczyk, N. R. Heckenberg, H. Rubinsztein-Dunlop, *J. Opt. A: Pure Appl. Opt.* **2007**, 9, S196.
- [32] G. Bosma, C. Pathmamanoharan, E. H. A. de Hoog, W. K. Kegel, A. van Blaaderen, H. N. W. Lekkerkerker, *J. Colloid Interface Sci.* **2002**, 245, 292.
- [33] S. J. Ivell, R. P. A. Dullens, S. Sacanna, D. G. A. L. Aarts, *Soft Matter* **2013**, 9, 9361.
- [34] S.-H. Lee, Y. Roichman, G.-R. Yi, S.-H. Kim, S.-M. Yang, A. van Blaaderen, P. van Oostrum, D. G. Grier, *Opt. Express* **2007**, 15, 18275.
- [35] J. Fung, K. E. Martin, R. W. Perry, D. M. Kaz, R. McGorty, V. N. Manoharan, *Opt. Express* **2011**, 19, 8051.
- [36] S. K. Sainis, V. Germain, C. O. Mejean, E. R. Dufresne, *Langmuir* **2008**, 24, 1160.
- [37] J. C. Crocker, D. G. Grier, *J. Colloid Interface Sci.* **1996**, 179, 298.
- [38] E. Nes, N. Ryum, O. Hunderi, *Acta Metall.* **1985**, 33, 11.
- [39] G. Gottstein, L. S. Shvindlerman, *Boundary Migration in Metals: Thermodynamics, Kinetics, Applications*, CRC Press, Boca Raton, FL, USA, **1999**.